CORE
Metadata, citation and similar papers at core.ac.uk
Provided by Digital library of Brno University of Technology

Time-Scale Domain Characterization of Time-Varying Ultrawideband Infostation Channel

Uche A. K. CHUDE-OKONKWO[1], Razali NGAH[1], Chee Y. LEOW[2], Tharek Abd RAHAMAN[1]

[1] Wireless Communication Center, Faculty of Electrical Eng., Univ. Teknologi Malaysia, Malaysia, 81310, UTM, Johor
[2] Dept. of Electrical & Electronic Engineering, Imperial College London, UK.

uche@utm.my, razalin@fke.utm.my, bruceleow@imperial.ac.uk, tharek@utm.my

Abstract. *The time-scale domain geometrical-based method for the characterization of the time varying ultra-wideband (UWB) channel typical of an infostation channel is presented. Compared to methods that use Doppler shift as a measure of time-variation in the channel this model provides a more reliable measure of frequency dispersion caused by terminal mobility in the UWB infostation channel. Particularly, it offers carrier frequency independent method of computing wideband channel responses and parameters which are important for ultrawideband systems. Results show that the frequency dispersion of the channel depends on the frequency and not on the choice of bandwidth. And time dispersion depends on bandwidth and not on the frequency. It is also shown that for time-varying UWB, frame length defined over the coherence time obtained with reference to the carrier frequency results in an error margin which can be reduced by using the coherence time defined with respect to the maximum frequency in a given frequency band. And the estimation of the frequency offset using the time-scale domain (wideband) model presented here (especially in the case of multiband UWB frequency synchronization) is more accurate than using frequency offset estimate obtained from narrowband models.*

Keywords

Ultrawideband, time-scale, geometrical model, time-varying, coherence time, frequency offset.

1. Introduction

The concept of infostation [1 - 3] presents a new way to look at the problem of providing high data rate wireless access. It is an isolated pocket area with small coverage (hundreds of meters) of high bandwidth connectivity that collects information requests from mobile users and delivers data while users are going through the coverage area. Infostations can be located in heavily populated areas such as the airport, shops, pubs, hotels, and along the highway. To cover larger area in the case of the highway, the infostation is positioned at intervals along the path.

Consider a scenario in which a user inside a vehicle moving along the highway desires to receive/transmit large chunk of data from/to an infostation network located along the highway as shown in Fig 1. This will require a technology that will be able to handle high data rate information transfer. Since, the infostation technology is designed for small area of coverage, low power transmission requirement is necessary in order to avoid interference with other existing services. One of the technologies that have the potential to deliver the envisaged high-data rate infostation services is the UWB signalling [3], [4]. The UWB has the basic attributes of extremely low transmission power, operating at unlicensed frequency, high data rate, multipath immunity and low cost. Hence, the characterization of the UWB channel for a typical infostation scenario is a necessity.

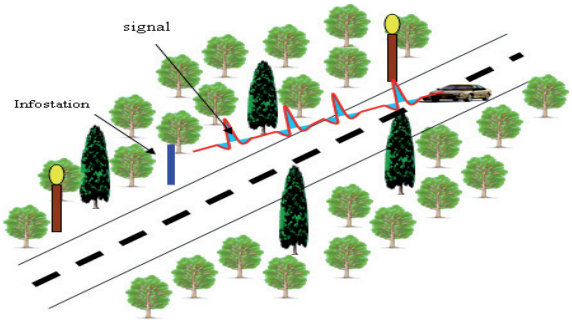

Fig. 1. Illustration of infostation wave propagation channel.

There are few existing articles [5], [6] on the infostation channel characterization. In [5], propagation models for different scenarios of short-range infostation wireless channels using a blend of deterministic and stochastic model were presented. Continuous wave measurements at 5.3 GHz were taken to determine the signal gain as a function of receiver position. But the frequency and time dispersions of the infostation channel were not addressed. In [6], the results from UWB outdoor measurement campaign were presented. The target scenario for measurement was a gas station, an environment envisioned in the context of UWB-based infostation. Frequency dispersion as a result of terminal mobility was not discussed. Instead, the use of virtual antenna array was employed to define an algorithm for the detection of scatterers' locations. However, for many infostation scenarios, time variation is expected due

to the mobility of one of the communication terminals/scatterers. Hence, the existing channel models cannot be used to describe this new target scenario where terminal mobility is expected.

In general terminal mobility translates to frequency dispersion. And frequency dispersion of a wireless channel is parameterized by the coherence time associated with that particular channel. The coherence time is obtained from the Doppler spread estimated from the scattering function [7]. When Doppler shift is used as the measure of the frequency dispersion, it is presumed that composite signals or subcarriers passing through the channel, experience the same amount of frequency shift obtained with respect to the center frequency. For narrow bandwidth composite signals, this approximation may be practically true and sufficient. However, for the UWB with large bandwidth (typically 500 MHz and above), the Doppler approximation wholly fails because the composite signals experience different Doppler shifts. Therefore, in the case of time-varying infostation channel, we ask the question; *1) is there a method of obtaining the wideband spreading function independent of the center frequency*?

To obtain the spreading function that is appropriate for any given channel model, appropriate eigenfunction must be defined. In order to incorporate time varying effects in the wideband channel model, the use of the singularity dirac function [6] as eigenfunction will be inappropriate due to the time-scaling property of a dirac function; scaling the dirac function simply varies the amplitude and not the frequency/scale value. Moreover, the use of the dirac function is not appropriate for the representation of propagation phenomena like diffraction and scattering [8]. Hence, we ask the question; *2) are there compact eigenfunctions with scaling ability and equivalent eigenstructure to model the time-varying UWB infostation channel*?

The above questions 1) and 2) can be addressed by time-scale domain channel characterization method presented in [9-11]. This method provides scalable eigenfunctions that can model the time-varying effect of the UWB infostation channel. The time-scale model offers compact eigenfunctions (wavelets) similar to the conventional UWB signaling waveform. The replacement of the dirac with wavelet is supported by [12]. The time-scale model also employs the time scaling operator which is independent of carrier frequency, to measure the frequency dispersion of the channel [11].

To model the time-scale domain channel, various types of propagation models can be employed. One of the propagation models that are widely used for wireless channel characterization is the geometric channel model (GCM). The GCM is well suited for simulations requiring a complete model of the channel due to its ray-tracing nature. However, the accuracy of a chosen GCM depends on how well the shape, size and scatterer distributions represent the physical channel. The short propagation distance and the low height of both the transmitting and receiving antennas in the infostation setting [5] allow for the use of geometrically based elliptical channel model [13-15] for the characterization of the propagation effects in the channel. By defining two heuristic rules termed bijective mapping rule and tapering-off normalized space-dependent intensity measure rule, it was shown in [13] that the geometrical-based single bounce elliptical model (GBSBEM) [14] abides by both rules. Thus, it is a good approximation to the physical reality from a wave propagation point of view. The GBSBEM is originally developed for narrowband/wideband channels and assume fixed antenna configuration [15]. The model was also considered in developing a planar wideband directional channel model applicable to UMTS micro-cells [16]. Its application to the UWB channel has been limited due to the complexity of such model since the frequency dependence of the various channel phenomena have to be taken into account. In [17] a 3-D space model was introduced which considered this frequency dependency. However, time-variation was not taken into account in the 3D model. Hence, the GCM-based time-varying UWB infostation channel characterization using appropriate equivalent ultrawideband eigenstructure is required. We also note the classical works of Qui [12], [18] on UWB propagation channel model which emphasize on the frequency characteristics and physics-based analysis of the UWB propagation channel.

In this work, we present the modified GBSBEM model in time-scale domain appropriate for the time-varying UWB infostation channel. This model is based on the integration of the time-scale domain channel model and the GBSBEM. The frequency dependency of the propagation phenomena is taken into account by means of the frequency dependent path-loss model. The time and frequency variation of the channel is quantified using the coherence time and root-mean square delay spread, respectively, obtained from the delay-scale spectrum function at different frequencies and bandwidths. In the context of traditional UWB, the channel is considered to be frequency selective, while it is considered to be flat in the context of the MB-OFDM.

2. Continuous Time-Scale Channel Characterization

The continuous time-scale representation of the linear time-varying (LTV) wideband channel $\mathbf{H}$, can be given by [11]:

$$y(t) = \iint \mathcal{U}_{\mathbf{H}}(\tau, s)\ a(t)\, x((t-\tau)/s) d\tau s^{-2} ds \tag{1}$$

and the time-frequency representation by [7]:

$$y(t) = \iint \mathcal{S}_{\mathbf{H}}(\tau, \upsilon)\ x(t-\tau) e^{j2\pi\upsilon t} d\tau d\upsilon \tag{2}$$

where $x(t)$ and $y(t)$ are the transmitted and received signals, respectively, and the term $a(t)$ is the attenuation. The terms $\mathcal{U}_{\mathbf{H}}(\tau, s) = \int y(t)\ a(t)\ x\left((t-\tau)/s\right) dt$ and $\mathcal{S}_{\mathbf{H}}(\tau, \upsilon) =$

$\int h(\tau,t)\, e^{-j2\pi\upsilon t}\, dt$ denote the delay-scale (wideband) spreading function [10], [11], [19] and the delay-Doppler spreading function [7], [19], respectively. While the latter is interpreted as the reflectivity of the scatterers associated to propagation delay τ and Doppler shift υ, the former is interpreted as the reflectivity of the scatterers associated to delay τ and scale shift (or time scaling) s. All integrals in this work are taken over the range [-∞ ∞] unless otherwise stated.

The relationship between scale shift and Doppler shift is given by: $s\{f_p\} = \{f_p\}\left((c \mp v)/(c \pm v)\right), \quad p = 1,2,3....,P$ where c and v are the speeds of the electromagnetic wave and the mobile antenna unit, respectively, and $\{f_p\}$ is the frequency vector comprising stepwise of all the frequency components of the system under consideration. The term $\{f_p\}$ can be approximated to the carrier frequency f_c in narrowband applications. However, for UWB applications $f_c \neq \{f_p\}$ and (2) is not an appropriate channel representation.

The delay-scale spectrum (D-SS) which indicates the relative contribution of the energy of the received signal at a specific delay and scale is given by: $\mathcal{H}(\tau,s) = |\mathcal{U}_{\mathrm{H}}(\tau,s)|^2$. The surface of $\mathcal{H}(\tau,s)$ emphasizes the delay and scale of the dominant energetic features in the received signal and is encompassed within the region $[\tau_{\min}\ \tau_{\max}]\times[\ s_{\min}\ s_{\max}\ ]$. The terms $s_{\min}$ and $s_{\max}$ are the minimum and maximum scale spreads, respectively, and, $\tau_{\min}$ and $\tau_{\max}$ are the minimum and maximum delay spreads, respectively. The power delay profile (PDP) and the scale spectrum are given by $\mathcal{H}(\tau) = \mathcal{H}(\tau,s)\big|_{s=1}$ and $\mathcal{H}(s) = \mathcal{H}(\tau,s)\big|_{\tau=0}$, respectively. The root mean squared (rms) delay spread τ_{rms} represents the standard deviation of the PDP and is given by:

$$\tau_{rms} = \left(\left(\int (\tau-\tau_m)^2 \mathcal{H}(\tau)\, d\tau\right)\left(\int \mathcal{H}(\tau)\, d\tau\right)^{-1}\right)^{1/2} \qquad (3)$$

where $\tau_m = \left(\int \tau\mathcal{H}(\tau)\, d\tau\right)\left(\int \mathcal{H}(\tau)\, d\tau\right)^{-1}$ is the mean delay.

The τ_{rms} and coherence time $T_c = 2/5\alpha$ where $\alpha = |1\text{-}s_{\max}|\{f_p\}$, are the values that indicate the channel dispersion in time and frequency, respectively. An important point to note is that the realization of $\mathcal{U}_{\mathrm{H}}(\tau,s)$ is independent of the carrier frequency or any reference frequency but depends basically on the velocity of the mobile terminal. Thus, different values of T_c can be obtained from a single realization for different values of frequencies. To compute the D-SS and subsequently the delay/scale profiles, the knowledge of the attenuation, delay and scale characteristics of the respective multipath is required. We can obtain these characteristics using the geometric elliptical channel model modified to include frequency characteristics.

3. Channel Model Description

3.1 Model Preliminaries

The GBSBEM presented here considers the geometric description of the spatial relationship among the infostation access point (IAP), scatterers and the mobile user equipment (MUE) within defined elliptical loops as shown in Fig. 2. It is assumed that wave propagation takes in the horizontal plane containing the tips of the transmitting and receiving antennas. The separation distance between the antennas is D. We note that although the GBSBEM is originally developed for the indoor channel, it can also be applied to the outdoor channel. In this context, the GBSBEM model proposed here considers an outdoor scenario in which case, the dimension of the outermost ellipse is taken with respect to the farthest possible scatterer(s) with significant influence.

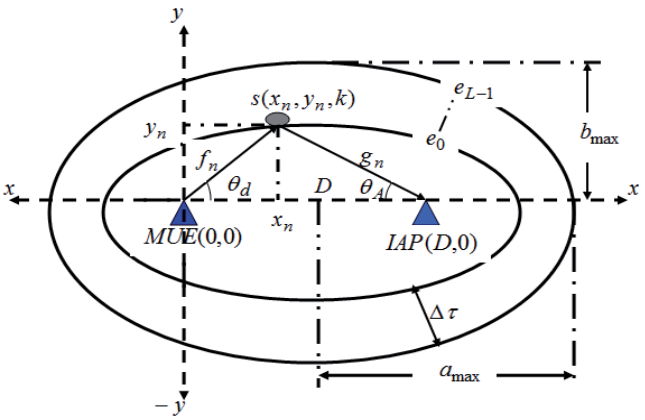

Fig. 2. Elliptical model for the UWB Infostation channel.

Each scatterer is defined as s in a hypothetical space-complex dielectric coordinate (x,y,e_l,k), where e_l l = 0,1,2..,L-1 is the specific elliptical loop within which the scatterers at global coordinate $s(x_n,y_n)$ with complex dielectric characteristics k lie. Let the xy coordinate system be such that the IAP is at the origin and the MUE lies on the x-axis. We assume that the communicating antennas are omnidirectional and of equal low heights which is typical of the infostation scenario. The typical radiation pattern of the antennas is shown in Fig. 3.

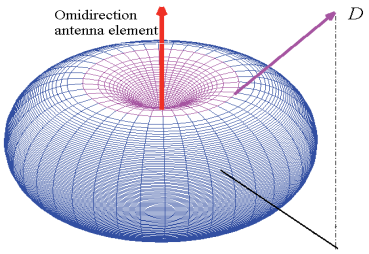

Fig. 3. Omnidirectional antenna radiation pattern.

We also make the following additional assumptions to those in [15]: 1) the scatterers may not have identical scattering coefficients, 2) the scatterers distributions (around the IAP and MUE) are assumed to follow known statistical distributions that are defined based on physical insight and mathematical tractability, 3) signals received at the *IAP* are plane waves propagating only along the azimuthal coordinate, and 4) for simplicity, each scatterer is an omnidirectional re-radiating element whereby the plane wave, on arrival, is reflected directly to the receiving antenna without the influence of other scatterers. Assumption 1) is justified by the fact that the potential scatterers include different objects like trees, concretes, steel, etc which have different dielectric properties; 2) is justified by the uneven/even, dense/sparse, and random placement of scatterers in different environments which will closely be matched by a known statistical distribution; 3) is justified by the fact that both antennas are approximately of the same height and; 4) is justified by the argument in [20] where multiple-scattering processes carry only low power.

For N number of scatterers at coordinates (x_n, y_n), $n = 1,2..,N$ and system bandwidth BW, the metric separation τ_Δ between two bi-centric ellipses e_i and e_j, $i, j \in l$ is given by: $\tau_\Delta = \xi c \Delta\tau$, where $\xi\Delta\tau = 1/(2BW)$ is the time delay resolution. The term $\xi \neq 0$ is the scaling factor which depends on the time scaling/ Doppler shift value of the MPCs associated with a particular delay. For most terrestrial wideband communication channels, $\xi \approx 1$ and we assume so here. This assumption is valid since the Doppler shift values often encountered in terrestrial wideband communication are far less than the operating BW, hence, $1/(2\xi BW) \approx 1/(2BW)$. So, while n = 1,2,…,N determines the overall number of propagation paths, l = 0,1,2..,L-1 defines the number of resolvable paths.

All MPCs received from scatterers within the same elliptical separation $\tau_\Delta^{(e_l)}$ have the same delay. However their path gains may crucially vary due to the intrinsic electromagnetic properties of the associated scatterers which define the scattering coefficients.

The ellipse has major axis half-length $a_l = 0.5\, cl\,\Delta\tau$ and minor axis half-length $b_l = 0.5 \times \sqrt{(cl\,\Delta\tau)^2 - D^2}$. The maximum delay $\tau_{\max} = (L-1)\Delta\tau$ occurs at the boundary of the biggest ellipse of consideration e_{L-1} for which $a_{L-1} = a_{\max}$ and $b_{L-1} = b_{\max}$. Thus all MPCs that arrive after $\tau_{\max}$ are considered insignificant.

The scatterer density $\Psi(x_n, y_n)$ is given by $\Psi(x_n, y_n) = 1/A_e$, where A_e is the area of the ellipse. The path length R from $MUE(0,0)$ to $IAP(D,0)$ through $s(x_n, y_n, k)$ is given by: $R_n^{(e)} = f_n + g_n$, where $f_n = \sqrt{x_n^2 + y_n^2}$ and $g_n = \sqrt{y_n^2 + (D - x_n)^2}$ are depicted in Fig. 2.

The probability density function (pdf) $\Psi_{\theta_d}(\theta_d)$ of the time-of-arrival (TOA) and the angle-of-arrival (AOA) as seen from IAP are given in general by [14]:

$$\begin{aligned}\Psi_{\theta_d}(\theta_d) &= \int_0^{f_m} \Psi_{\tau,\theta_d}(\tau,\theta_d)\, d\tau \\ &= \frac{1}{8\pi a_{\max} b_{\max}} \left(\frac{D^2 - \tau^2 c^2}{D\cos\theta_d - \tau c} \right) \Psi_{x,y}(f\cos\theta_d, f\sin\theta_d)\end{aligned} \tag{4}$$

where $f_m = (D^2 - 4a^2)\,(2(D\cos\theta_d - \tau c))^{-1}$, θ_d is the AOA, τ is delay, c is the speed of electromagnetic wave and $\Psi_{x,y}(.)$ is the scatterer density function.

The TOA p.d.f. can be obtained from the expression:

$$\Psi_\tau(\tau) = \frac{1}{A_e} \frac{d}{d_\tau} A_r(\tau) \tag{5}$$

where A_r is the intersection of the scatterer region with respect to the ellipse of area A_e.

By making appropriate choice with regards to the statistical distribution of scatterers, (4) and (5) can be simplified further.

3.2 Scatterer and Complex Dielectric Distributions

The use of GSBEM involves randomly placing scatterers inside an elliptical region according to a spatial probability density function. The spatial distribution of the scatterers can be defined using an appropriate known statistical distribution functions. The choice of the distribution follows the physical description and positioning/dimension of the scattering objects within the propagation environment. The appropriate statistical distribution for a particular area can be obtained by extensive study of the related environment. The use of the right distribution for a specific channel is important since the accuracy of the model depends on it. There are yet no numerical data that provide such information on scatterer distribution in diverse environment. Since there is generally a line-of-sight (LOS) MPC, for the purposes of this work, we choose the uniform distribution considered in [21] and which was also assumed in [22] for the statistical analysis of a mobile-to-mobile Rician fading channel model.

By assuming uniform distribution of scatterers, it implies that $\Psi_{x,y}(f\cos\theta_d, f\sin\theta_d) \approx 1$, hence (4) becomes:

$$\Psi_{\tau,\theta_d}(\tau,\theta_d) = \frac{\left(D^2 - \tau^2 c^2\right)\left(D^2 c + \tau^2 c^3 - 2\tau c^2 D\cos\theta_d\right)}{4A\left(D\cos\theta_d - \tau c\right)^3} \tag{6}$$

And the pdf of the AOA is then given by:

$$\Psi_{\theta_D}(\theta_d) = \frac{1}{8\pi a_{\max} b_{\max}} \left(\frac{\tau_{\max}^2 c^2 - D^2}{\tau_{\max} c - D\cos\theta_d} \right). \tag{7}$$

From the assumption of uniform distribution, the TOA pdf can then be computed by assuming that $A_r(\tau)$ is the area of the ellipse itself. Thus $A_r(\tau) = 0.25\pi\tau c\sqrt{c^2\tau^2 - D^2}$ and $A_e = \pi a_{\max} b_{\max}$. Hence:

$$\Psi_\tau(\tau) = \frac{c}{4a_{\max}b_{\max}} \cdot \frac{2c^2\tau^2 - D^2}{\sqrt{c^2\tau^2 - D^2}}. \quad (8)$$

Of course, different statistical distributions yield different pdfs for both AOA and TOA.

Although the scatterers' coordinate positions are frequency independent, their respective influence on the channel response is frequency dependent. This dependency is a function of their respective permittivity, permeability and conductivity. Each scatterer is defined by a particular value of complex dielectric constant. The dielectric constant value of a scatterer defines the ratio of the transmitted signal power to that of the reflected signal (towards the receiving antenna). Since there are numerous scatterers in the environment, statistical distribution can be used to approximate the placement of scatterers with definitive complex dielectric constant values inside the ellipse. In some channels, scatterers with dielectric constant values that are within close range can be dominant, while in some channel the distribution is more uniform. For this work, we consider the highway environment with the complex dielectric constant values of most scatterers represented as those of wet wood (trees). Few scatterers (lamp posts) have complex dielectric values of good conductors. The distribution of the scatterers' dielectric constants greatly influences the received power and subsequently the response of the channel.

3.3 Frequency Dependent Characteristics

In narrowband and wideband geometrical channel models, the frequency characteristics of the scatterers are often neglected. However, in UWB, in order to obtain a more accurate channel description, the frequency characteristics of the scatterers should be taken into consideration.

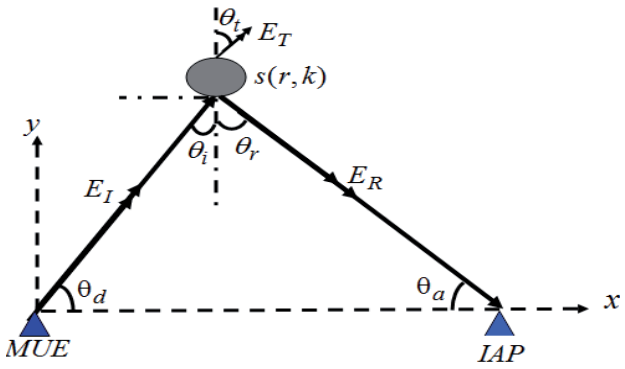

Fig. 4. Illustration of reflected and transmitted waves for wave incident upon a scatterer at oblique angle (E_R and E_T are the reflected and transmitted waves, respectively).

Let us consider a homogenous linearly polarized plane wave E_I at oblique incidence on a scatterer at location r for perpendicular polarization as shown in Fig. 4.

$$E_I(r) = E_o e^{-jk_1 z.r} \quad (9)$$

where E_o and z are the amplitude and direction of travel of the incidence wave, respectively. The term k_1 is the complex dielectric constant of free-space.

In general, if we assume that the different media are isotropic which is approximately true for most materials influencing mobile radio wave propagation, then:

$$k_q = \varepsilon(f) - j\sigma(f)/(\omega\varepsilon_o), \quad q = 1,2,3....Q \quad (10)$$

where $\varepsilon(f)$ is frequency dependent product of the free-space dielectric constant ε_o and the relative dielectric constant ε_r of the particular medium indexed by q, σ is the conductivity, and $\omega = 2\pi\{f_p\}$ is the composite frequency of consideration in radian. Since numerical estimates of dielectric constants and conductivity of materials at different frequency has not been provided as yet, the frequency-dependence of k_q is taken into account by ω. Hence (10) becomes:

$$k_q = \frac{\omega\varepsilon_{f_R}\varepsilon_o - j\sigma_{f_R}}{\omega\varepsilon_o} \quad (11)$$

where $\varepsilon(f) = \varepsilon_{f_R} = \varepsilon_o\varepsilon_r$ and $\sigma(f) = \sigma_{f_R}$ are evaluated at some reference frequency f_R.

For a wave incident on the scatterer's surface at an angle Θ_i, the reflection coefficient $\Gamma_\perp$ can be given as:

$$\Gamma_\perp = \frac{\sqrt{k_2}\cos\Theta_i - \sqrt{k_1}\cos\Theta_t}{\sqrt{k_2}\cos\Theta_i + \sqrt{k_1}\cos\Theta_t} \quad (12)$$

where Θ_t is the angle of transmission (equivalent to angle of reflection). The terms k_2 is the complex dielectric constants of the scatterer.

If we consider waves propagating only along the azimuth, then it can easily be shown:

$$\Gamma_\perp = \frac{\sqrt{k_2}\cos(90-\theta_d) - \sqrt{k_1}\cos\Theta_t}{\sqrt{k_2}\cos(90-\theta_d) + \sqrt{k_1}\cos\Theta_t}. \quad (13)$$

Thus the magnitude of the reflected wave (at the point of incidence) E_R depends on the dielectric properties of both media. Let us denote the relative amount of energy flux reflected at the scatterer surface by:

$$\Lambda = \frac{\left|E_R \times H_R^*\right|}{\left|E_I \times H_I^*\right|} = \left(\frac{\sqrt{k_2}\cos(90-\theta_d) - \sqrt{k_1}\cos\Theta_t}{\sqrt{k_2}\cos(90-\theta_d) + \sqrt{k_1}\cos\Theta_t}\right)^2. \quad (14)$$

Since there can be no energy stored in the scatterers surfaces by virtue of the conservation of energy, it implies that the power transmission coefficient $T_\perp$ in relation to $\Gamma_\perp$ by:

$$T_{\perp} = 1 - \left(\frac{\sqrt{k_2}\cos(90-\theta_d) - \sqrt{k_1}\cos\Theta_t}{\sqrt{k_2}\cos(90-\theta_d) + \sqrt{k_1}\cos\Theta_t} \right)^2$$

$$= \frac{\sin(2(90-\theta_d))\sin 2\Theta_t}{\sin^2(\Theta_t + 90 - \theta_d)} \quad (15)$$

where $\Theta_t = \sin^{-1}\left(\frac{k_1}{k_2}\sin(90-\theta_d) \right)$.

We assume that the power transmission coefficient results from the transmitted wave and all other forms of power losses.

3.4 Frequency Dependent Path-Loss Model

Let us represent the scattering phenomenon as shown in Fig. 5. We assume that scatterer is impinged upon by a compactly supported signal like a Mexican hat wavelet:

$$E_I(t) = E_o(1-t^2)e^{-t^2} \quad (16)$$

where E_o has a power $P_o = 1$, and $t \in \Re$.

The transmitted signal $x(t) \equiv E_I(t)$ with power, P_T, experiences free-space path loss as it travels from the transmitter *Tx* to the scatterer's position marked $s(r,k)$. At the scatterer surface, we assume that only the electromagnetic wave reflection and transmission phenomena are involved. Hence, part of the signal incident upon the surface is reflected towards the receiver *Rx* and part is transmitted through the scatterer. The transmission coefficient accounts for power loss L_T, if we assume single bounce.

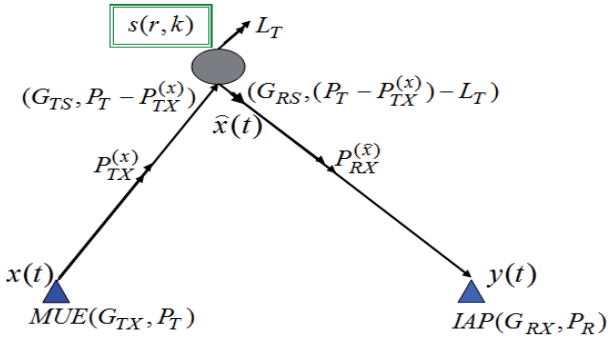

Fig. 5. Frequency dependent path-loss for the UWB channel.

Then the reflected signal $\hat{x}(t) \equiv E_R(t)$ experiences free-space path loss as it travels from the scatterer surface to the *Rx*. If we assume that the scatterer acts like an antenna (re-radiator), then the received signal power P_R is given by:

$$P_R(d,\{f_p\}) = \left\{ \left(P_T G_{TX} G_{RS} \left(\frac{c}{4\pi\{f_p\} d_1} \right)^2 \right)_x \Lambda(k,\{f_p\}) \right\} \cdot \left(G_{TS} G_{RX} \left(\frac{c}{4\pi\{f_p\} d_2} \right)^2 \right)_{\hat{x}} \quad (17)$$

where d is the path distance from *Tx* to *Rx*, d_1 path distance from *Tx* to scatterer surface, d_2 path distance from scatterer surface to *Rx*, G_{TX} transmitting antenna gain, G_{RX} receiving antenna gain, G_{TS} gain of the scatterer surface when assumed to act like a transmitting antenna, G_{RS} gain of the scatterer surface when assumed to act like a receiving antenna, $\Lambda(k,f)$ reflected power coefficient at the scatterer surface.

If we assume that $G_{RS} = G_{TS}$, then denoting the scatterer gain by $G_S = G_{TS} = G_{RS}$, we have:

$$P_R(d,\{f_p\}) = P_T G_{TX} G_{RX} G_S^2 \left(\frac{c}{4\pi\{f_p\}} \right)^4 \left(\frac{1}{d_1 d_2} \right)^2 \cdot \Lambda(k,\{f_p\}) G_{TS} G_{RX} \left(\frac{c}{4\pi\{f_p\} d_2} \right)^2. \quad (18)$$

We do not consider shadowing since the locations of the infostation and the mobile transceiver are close to each other and LOS path is always present [5]. Hence, for each elliptical area the power P_R associated with each propagation delay is given by the summation of the respective powers of each associated component scatterer:

$$P_{R,\tau} = \sum_{u=0}^{U-1} \left(P_{R,\tau,u} \right), \quad u = 0,1,2,\ldots,U-1 \quad (19)$$

where $U \le N$ is the number of scatterers inside a given elliptical area.

3.5 Time Scaling

Having obtained the delay and AOA using the model described in the previous section, the time scaling associated with each scatterer at a particular elliptical loop defined by $l\tau_\Delta$ is computed using the AOA:

$$s = 1 \pm \frac{2v}{c}\cos(\theta_d) \quad (20)$$

where v is the velocity of the MUE.

When more than one scatterer is inside an elliptical area, the scatterer associated with the maximum scale spread value is used to represent the scale at that particular elliptical loop. This value is the scale value for the corresponding delay $\tau = l.\Delta\tau$ at that ellipse. In order to obtain the Doppler spread υ at any particular frequency of interest, the relationship between the Doppler spread and time scaling is $\upsilon = (1-s)\{f_p\}$.

4. Numerical Results and Discussion

Let us consider a typical infostation communication scenario like that in Fig. 1. The signaling function is assumed to be the same function given in (16). We assume that the power P_T and duration T_{pulse} of this function is

about 100 mW and 10 ns, respectively. The following parameters are defined for this simulation; N = 5000, D = 25 m, a_{max}= 33 m, b_{max}= 12 m, v = 10 m/s, $\varepsilon_r(tree) = 30$, $\varepsilon_r(lamp\ post) = 1000$, $\sigma(tree) = 100\ \Omega m$, and $\sigma(lamp\ post) = 3.7 \times 10^2\ \Omega m$. All antenna gains in (17) are assumed to be unity. The delay and AOA are obtained using the model in Section 3. For mobile velocity of v the scale is computed using (20). The T_c and τ_{rms} are obtained from the D-SS which is computed using (1). The D-SS for 528 MHz bandwidth at the frequency of 3.1, 3.628 and 4.28 GHz are shown in Fig. 6 - 8, respectively.

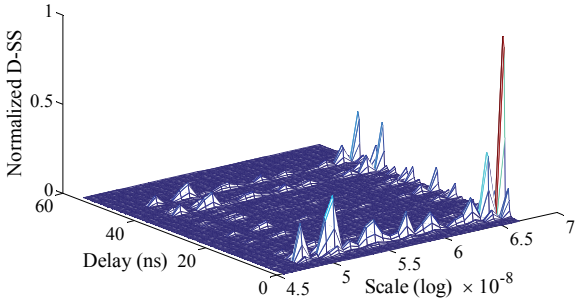

Fig. 6. D-SS at 3.1 GHz for a bandwidth of 528 MHz.

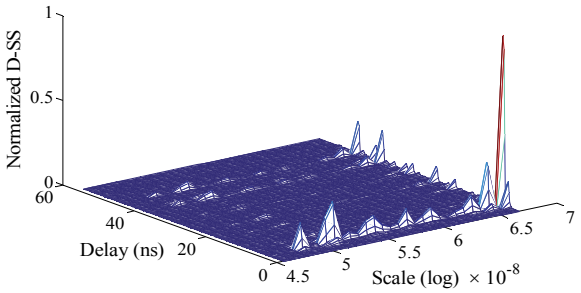

Fig. 7. D-SS at 3.628 GHz for a bandwidth of 528 MHz.

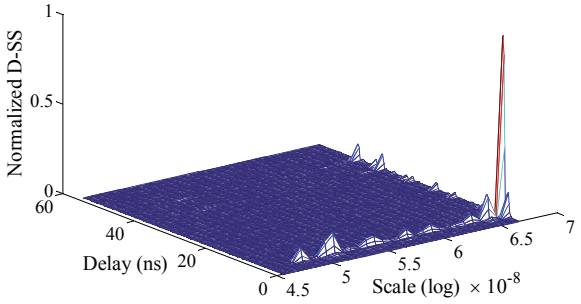

Fig. 8. D-SS at 4.28 GHz for a bandwidth of 528 MHz.

It can be seen from Fig. 6 - 8, that the dominant MPC is the LOS component. The magnitude of the D-SS varies with frequency; a phenomenon that is closely associated with the dependency of scattering coefficients on frequency. Thus, as frequency increases more energy is lost.

The results in Fig. 9 are obtained for fixed bandwidth over a frequency range that can be taken anywhere from 3.1-9.6 GHz. From the graph, it is obvious that at lower bandwidth the variation in τ_{rms} with frequency is not so significant compared to the case of higher bandwidths. By changing the bandwidth, the resolution of the delay is changed, resulting in the variation of τ_{rms} across bandwidth. This is so since the number of delay bin is proportional to the bandwidth under consideration. The cumulative distribution function (cdf) of the delay spread at different frequencies and different bandwidths are shown in Fig. 10. The plots in Fig. 10 indicate that variation in delay spread is independent of frequency but dependent on bandwidth. The plot of coherence time at different frequencies for BW=528 MHz is shown in Fig. 11.

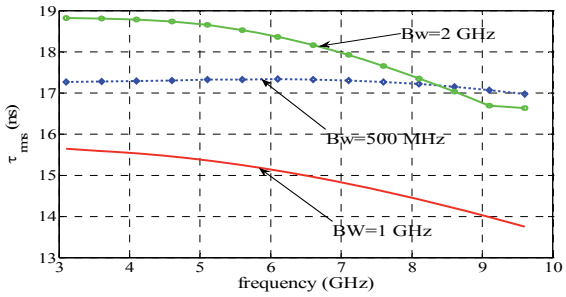

Fig. 9. RMS delay spread at different frequencies and BW.

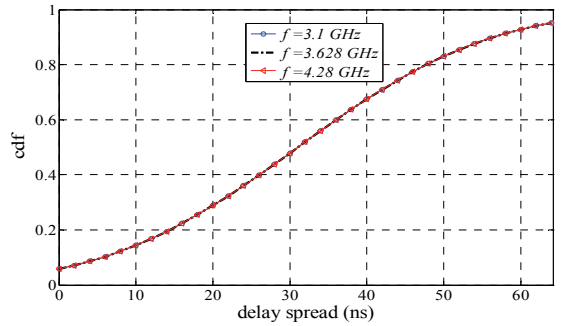

(a)

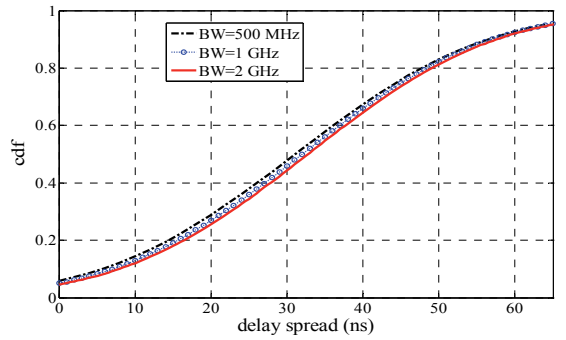

(b)

Fig. 10. The cdf of delay spread at (a) different frequencies, (b) different bandwidths.

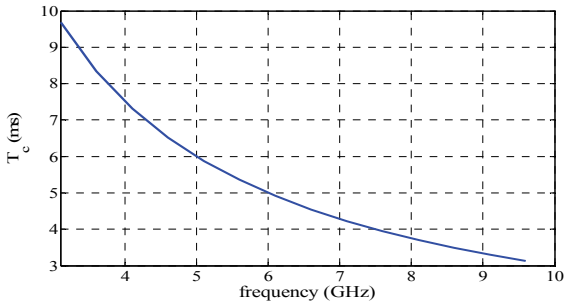

Fig. 11. Coherence time at different frequencies for BW = 528 MHz.

Fig. 11 shows the expected variation of T_c with frequency at a bandwidth of 500 MHz. The same values are obtained at bandwidths 1 GHz and 2 GHz. Hence, within a given bandwidth, T_c varies with frequency, but is independent of the change in bandwidth. This can be explained by the fact that T_c does not depend on bandwidth but frequency. For the bandwidth of approximately 500 MHz and frequency ranges 3.1-3.6 GHz, 5.0-5.5 GHz and 10.0-10.5 GHz, the variation of T_c with frequency is shown in Tab. 1, Tab. 2 and Tab. 3, respectively.

				f_c			
f (GHZ)	3.1	3.2	3.3	3.35	3.4	3.5	3.6
T_c (ms)	9.68	9.36	9.09	8.96	8.82	8.57	8.33

Tab. 1. T_c vs f at 3.1-3.6 GHz.

				f_c			
f (GHZ)	5.0	5.1	5.2	5.25	5.3	5.4	5.5
T_c (ms)	6.00	5.88	5.77	5.71	5.66	5.56	5.46

Tab. 2. T_c vs f at 5.0-5.5 GHz.

				f_c			
f (GHZ)	10.0	10.1	10.2	10.25	10.3	10.4	10.5
T_c (ms)	3.00	2.97	2.94	2.93	2.92	2.89	2.86

Tab. 3. T_c vs f at 10.0-10.5 GHz.

In order to see the merit in characterizing a wideband channel in the time-scale domain, take the case of Tab. 1. In this table, the values of T_c at different frequencies within the same operational bandwidth that span from 3.1 GHz to 3.6 GHz are shown. In the time-frequency regime where the channel delay-Doppler spectrum is obtained with reference to the center frequency f_c, the value of T_c is 8.96 ms. This value defines the frame length of the transmission over which the channel response is invariant. With respect to the maximum frequency f_{max} which in this case is 3.6 GHz, it implies that the channel varies over the duration given by the difference between T_c at f_{max} and T_c at f_c. This increases the error margin and will affect the performance of the channel estimation algorithm used. As an example, we consider the transmission of $Z_0 = T_{c,fc} / T_{pulse}$ symbols within a frame of length $T_{c,fc}$ (meaning T_c at f_c). The first 500 symbols are used as the training sequence. The ideal (conventional) scenario is that the channel is invariant over this frame length ($T_{c,fc}$). However, in reality the number of symbols that actually experience channel invariance is $Z_1 = T_{c,fmax}/T_{pulse}$ where $T_{c,fmax}$ means T_c at f_{max}. Here, we assumed that the channel (filter) is [0.86 0.66 0.27 0.1+j0.2] for the duration over which the channel is invariant ($T_{c,fmax}$), and [0.85 0.65 0.28 0.1+j0.3] for the duration over which the channel varies ($T_{c,fc} - T_{c,fmax}$). The channel estimation is done using least-mean-square (LMS) algorithm. And the signal error rate (SER) of quadrature phase-shift keying (QPSK) that illustrates this increase in error margin for the cases of Tab. 1 is shown in Fig. 12. It can be seen from Fig.12 that the SER performance is better when the frame size is defined using the T_c = 8.33 ms obtained at the highest frequency f_{max} than that obtained at f_c .

Another obvious merit of the method presented here is the issue of frequency synchronization in multiband UWB (MB-UWB). Here it is important that the frequency offset estimation be done bearing in mind the discrepancy in Doppler spread across the subcarriers. Let us consider the case where the subcarriers are separated by 528 MHz and span 3.1-9.6 GHz. If we assume a perfect frequency offset estimation from the delay-Doppler/delay-scale spectrum, then the loss in signal-to-noise ratio (SNR) that results while assuming offset around f_c (the case of frequency offset estimation using delay-Doppler spectrum) is shown

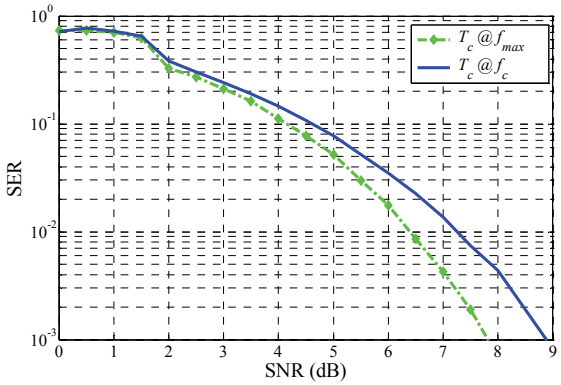

Fig. 12. SER for channel estimation with respect to T_c at f_c Tc and T_c at f_{max}.

in Fig. 13. It can be seen from Fig. 13 that as bandwidth increases, the SNR loss variance increases for a given SNR. Hence, for narrowband the SNR loss is approximately even at all subcarrier frequencies, hence the variance is very low. This implies that the assumption of an even frequency offset across the subcarriers of the narrowband OFDM system, suffices. However, for wideband the SNR loss variance is high. This implies that in MB-UWB, instead of assuming offset around f_c, frequency offset estimation should be done be considering a scale offset from which frequency offsets at different frequencies can be estimated. An idea close to the one presented above, in terms of offset frequency estimation has been presented in [23]. However, unlike [23], the discussion above does not assume even time scaling in all

propagation paths which is justifiable in time-varying UWB channels.

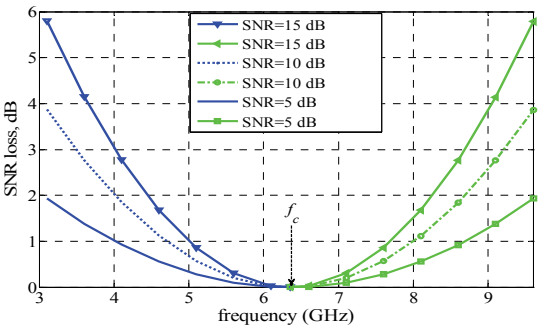

Fig. 13. Effect of offset frequency estimation error in MB-OFDM.

5. Conclusion

This paper presents a geometrical-based characterization of the time-varying UWB channel in the time-scale domain. This type of channel is typical of the infostation channel a technology that is envisaged to providing high data rate wireless access in areas like along the highway. Unlike the conventional UWB models, the time-scale domain provides an eigenstructure that is suitable for representing both the frequency variations encountered in such channel. The channel response in the form of delay-scale spectrum is used to estimate the channel parameters (coherence time, scale spread and rms delay spread). The method of obtaining the D-SS is independent of the center frequency; hence a single realization can be used to obtain channel parameters at a chosen frequency of operation. Results show that the frequency dispersion of the channel depends on the frequency components in a given bandwidth, but does not depends on the choice of bandwidth. And time dispersion depends on bandwidth and not on the frequency. Defining the frame length for traditional UWB using the maximum frequency in a given wide bandwidth of consideration gives a better error performance compared to that obtained in the case where the frame length is defined at the center frequency. It was also shown that the estimation of the frequency offset from the D-SS for synchronization in multiband UWB is more accurate than that using estimate centered on the center frequency.

Acknowledgements

The authors thank the Ministry of Higher Education (MOHE), Malaysia for providing financial support for this work through the Grants (4D040 and Q.J130000.7123.02H31) managed by the Research Management Center (RMC), Universiti Teknologi Malaysia (UTM). We also thank the reviewers of this manuscript for their constructive remarks.

References

[1] GALLUCIO, L. et al. Timely and energy-efficient communications in rural infostation systems. *IEEE Wirel. Commun*., June 2008, p. 48-53.

[2] RAJAPPAN, G., ACHHARYA, J., LIU, H., MANDAYAM, N., SESKAR, I., YATES, R. Mobile infostation network technology. In *Proc. SPIE on Wireless Sensing and Processing*. Orlando (USA), 2006.

[3] CHOWDHURY, H., MEKELA, J. P., PAHLAVAN, K. Statistical information transfer in random crossing of infostation coverage. In *Proc. 2005 Finnish Signal Processing Symposium*. Kuopio (Finland), August 2005.

[4] LAKKUNDI, V. Ultra wideband communication: History, evolution and emergence. *Acta Polytechnica,* 2006, vol. 46, no. 4, p. 18-20.

[5] DOMAZETOVIC, A., et al. Propagation models for short-range wireless channels with predictable path geometries. *IEEE Trans Commun*., July 2005, vol. 53, no.7, p.1123-1126.

[6] SANTOS, T., et al. Modeling the ultra-wideband outdoor channel: measurements and parameter extraction method. *IEEE Trans. Wirel. Commun*., Jan. 2010, vol. 9, no.1, p. 282-290.

[7] MOLISCH, A. F. *Wireless Communication*. England: John Wiley, 2005.

[8] McNAMARA, D. A., et al. *Introduction to the Uniform Geometrical Theory of Diffraction*. Boston: Artech House, 1990.

[9] RICKARD, S. T., BALAN, R. V., POOR, H. V., VERDU, S. Canonical time-frequency, time-scale, and frequency-scale representations of the time-varying channels. *International Press on Communication in Information & System*s, 2005, vol. 5, no. 2, p. 197-226.

[10] YE, J., PAPANDREOU-SUPPAPPOLA, A. Discrete time-scale characterization and wideband time-varying systems. *IEEE Trans. Sig. Proc*., 2006, vol. 54, no. 4, p. 1364-1375.

[11] CHUDE-OKONKWO, U. A. K., et al. Time-scale domain characterization of nonstationary wideband vehicle-to-vehicle propagation channel. In *Proc. IEEE APACE 2010*. Malaysia, 9-10 November, 2010, p.1-6.

[12] QUI, R. C. A study of the ultra-wideband wireless propagation channel and optimum UWB receiver design. *IEEE J. Sel. Areas Commun*., July 2002, vol. 20, no. 9, p. 1628-1637.

[13] CHEN, Y., DUBEY, K. Accuracy of geometric channel-modeling methods. *IEEE Trans. Vehic. Tech*., January 2004, vol. 53, no. 1, p. 82-93.

[14] ERTEL, R. B., REED, J. H. Angle and time of arrival statistics for circular and elliptical scattering models. *IEEE J. Select. Areas Commun*., November 1999, vol. 17, no. 11, p. 1829-1840.

[15] LIBERTI, J. C, RAPPAPORT, T. S. A geometrically based model for line of sight multipath radio channels. In *IEEE Vehicular Technology Conf*., Apr. 1996, p. 844-848.

[16] MARQUES, M. G., CORREIA, L. M. A wideband directional channel model for UMTS microcells. In *Proc.of IEEE PIMRC,* 2001.

[17] CHEN, Y., DUBEY, K. An azimuth-frequency domain geometric model for ultrawide bandwidth signal propagation. *Wirel. Pers. Commun*., 2004, vol. 31, no. 1-2, p. 1-18.

[18] QUI, R. C. A generalized time domain multipath channel and its application in ultra-wideband (UWB) wireless optimal receiver design-part II: physics-based system analysis. *IEEE Trans. Wirel. Commun.,* Nov. 2004, vol. 3, no. 6, p. 2312-2324.

[19] MATZ, G., HLAWATSH, F. Time-varying communication channels: fundamentals, resent developments, and open problems. Invited paper in *Proc. of 14th EUSIPCO-06*, Sept. 2006.

[20] SANTOS, T., et al. Modeling the ultra-wideband outdoor channel: model specification and validation. *IEEE Trans. Wirel. Commun*., June 2010, vol. 9, no. 6, p. 1987-1997.

[21] MITILINEOS, S. A., CAPSALIS, C. N., THOMOPOULOS, S. A. Simulation of small-scale fading in mobile channel models for next-generation wireless communications. In *Handbook of Research on Heterogeneous Next Generation Networking: Innovations and Platforms*, edited by Kotsopoulos, S. A. and Ioannou, K. G., Published by Information Science Reference, 2009.

[22] WANG, L. C, LIU, W. C., CHENG, Y. H. Statistical analysis of a mobile-to-mobile Rician fading channel model. *IEEE Trans. Vehic. Tech*., Jan. 2009, vol. 58, no. 1, p. 32-38.

[23] MASON, S. F., et al. Detection, synchronization, and Doppler scale estimation with multicarrier waveforms in underwater acoustic communication. *IEEE J. Sel. Areas in Commun*., Dec. 2008, vol. 26, no. 9, p. 1638-1649.